Available online at www.sciencedirect.com
SCIENCE DIRECT®
Journal of Magnetic Resonance 159 (2002) 190–194
JMR Journal of Magnetic Resonance
www.academicpress.com

Inductive shielding of NMR phase noise

E.E. Sigmund,[a,*] V.F. Mitrović,[a] E.S. Calder,[a] G.W. Thomas,[a] H.N. Bachman,[a] W.P. Halperin,[a] P.L. Kuhns,[b] and A.P. Reyes[b]

[a] *Department of Physics and Astronomy, Northwestern University, Evanston, IL, 60208, USA*
[b] *National High Magnetic Field Laboratory, Condensed Matter Physics NMR, Tallahassee, FL, 32306, USA*

Received 12 June 2002; revised 3 September 2002

Abstract

We report on a solution to the problem of phase noise in nuclear magnetic resonance (NMR) experiments. Phase noise refers to the variation in the phases of NMR signals from successive acquisitions due to an unstable applied field. Such a situation exists in high-field resistive Bitter magnets and, for sufficiently long timescales, can cause serious signal degradation upon signal averaging. An inductive shield, formed by a highly conducting metal tube placed around the sample and along the applied field, provides screening of the AC components of the applied field and thereby retains phase coherence over long periods. Although simple in principle there are technical difficulties for practical implementation of this method. We present demonstrations of the utility of this approach. In particular, we show a significant extension of the effective transverse coherence time of the ^{13}C resonance in doubly ^{13}C-labeled glycerol in a resistive Bitter magnet. This was accomplished through the use of a highly conducting aluminum shield, cooled to 4 K with liquid helium.

Keywords: Bitter magnet; Shielding; Phase noise

1. Introduction

Bitter magnets have provided access to the high magnetic field regime for numerous scientific experiments, including nuclear magnetic resonance (NMR), producing continuously applied fields of 30 T or higher. However, since the magnets are resistive and have low inductance, the field they generate suffers from temporal instability, as much as 10 ppm. For NMR experiments over sufficiently long timescales in which signal averaging is performed, this instability causes a variation in the phase of the transverse magnetization from one acquisition to the next. When such acquisitions are accumulated the net signal deteriorates. Previously, we have experimentally investigated this ''phase noise'' effect in a resistive Bitter magnet [1]. In order to perform any NMR measurement, which measures spin decoherence over timescales long compared with that of the magnet ripple (~60 Hz), such as spin–spin relaxation or diffusion measurements, the extrinsic decoherence due to signal averaging with phase noise must be eliminated. While extensive work has been done to successfully suppress magnetic field fluctuations by inductive feedback or NMR lock techniques [2], such methods are limited by the operational timescale of the feedback circuit, so higher frequency ripple components are not as well compensated. In this work we present results from an alternate method: a highly conducting cylindrical inductive shield. Such a low-pass filter will have an opposite frequency dependence to a feedback technique, and be optimized for higher frequencies. This should make it successful in the Bitter magnet case so long as the frequency scale of its shielding can be brought to the 60 Hz level, as we have shown in this work using a helium-cooled aluminum shield.

2. Shielding experiments

The use of inductive shielding in the Bitter magnet environment is challenging in numerous ways. First, the

* Corresponding author.
E-mail address: esigmund@northwestern.edu (E.E. Sigmund).

1090-7807/02/$ - see front matter © 2002 Elsevier Science (USA). All rights reserved.
PII: S1090-7807(02)00012-5

bore size of typical resistive magnets at the National High Magnetic Field Laboratory (NHMFL) in Tallahassee, Florida is only 32 mm. The minimal probe and cryostat size requirements in this space allow a maximal shield thickness of ~2.5 mm. With this geometrical restriction, we must maximize the conductivity of the shield to obtain sufficient screening in the 60 Hz range. This is done by cooling the shield to 4 K with liquid helium. Simultaneously, the NMR sample, only 1 cm away from the 4 K shield, must in some cases be held at or near room temperature. This second difficulty can be overcome with a vacuum space between the sample and the shield. Given these extreme conditions, a characterization of the shielding capability in the 60 Hz frequency range is desirable. Prior to the Bitter magnet experiment, we measured this capability in two ways: (1) inductive coupling measurements between two coaxial coils separated by shields of different resistivities and geometry, and (2) NMR experiments performed in a stable superconducting magnet with a superimposed harmonic field variation. Finally, we carried out NMR transverse relaxation measurements with a cooled shield in the Bitter magnet environment.

First we will present the measurement techniques employed to characterize a given shield's capability, then describe the analysis of this shielding data. The first technique of inductive coupling, sketched on the left in Fig. 1, consisted of a simple pickup measurement. An AC current $I = I_0 \cos(\omega t)$ was passed through the outer coil, and the amplitude of the induced voltage V_p on the inner coil was measured as a function of frequency ω. This measurement was performed both with and without a shield in place between the two coils. The ratio V_p/I_0 was used as a convenient parameter that was minimally dependent on the two coils. The shielding fraction S was experimentally determined by the ratio of the values of this parameter with and without the shield,

$$S_{\text{ind}} = \frac{(V_p/I_0)_{w/\text{shield}}}{(V_p/I_0)_{\text{noshield}}}. \tag{1}$$

The second method for measuring the shielding fraction was an NMR technique, sketched on the right in Fig. 1. As mentioned above, an NMR experiment performed with signal averaging in an unstable applied field will suffer a signal degradation with a time-dependence characteristic of the instability. The form this effect takes for a single-harmonic instability and a standard Hahn echo experiment can be calculated exactly [1]:

$$\left|\frac{M_t}{M_0}(2\tau)\right| = \left|J_0\left(4\frac{\gamma h}{\omega}\sin^2\left(\frac{\omega\tau}{2}\right)\right)\right|. \tag{2}$$

Here γ is the gyromagnetic ratio of the nucleus being measured, τ is the Hahn echo pulse separation, h and ω are the amplitude and frequency of the applied magnetic field ripple, and J_0 is the zeroth order Bessel function of the first kind. This well-defined decoherence form, once the intrinsic decoherence profile of a given sample has been measured and separated, provides a direct measurement of the field amplitude h seen by the nuclei at fixed frequency ω through a fit of the transverse magnetization profile. Fig. 1 shows such a fit for the ^{1}H resonance in glycerol at 3.15 T and an applied instability of 7.8 mG at 40 Hz. This measurement was carried out as a function of frequency both with and without a shield to measure the shielding fraction,

$$S_{\text{NMR}} = \frac{h_{w/\text{shield}}}{h_{\text{noshield}}}. \tag{3}$$

The results of these AC measurements were quantitatively consistent with independent shift measurements of the NMR resonance frequency with DC applied fields up to 80 mG. This means that at a known current, the dephasing profiles (e.g., right lower panel of Fig. 1) in the presence of the applied ripple can be fit with no adjustable parameters.

Two shields were used in this study; both were chosen and treated to maximize their conductivity. Their geometries are given in Table 1. One shield of oxygen-free, high conductivity (OFHC) copper was machined to the desired size, etched in nitric acid solution, and annealed in a 1 mtorr pure oxygen atmosphere at 928 °C for 47 h. The partial pressure of oxygen was introduced to allow internal oxidation of impurities. A second shield of

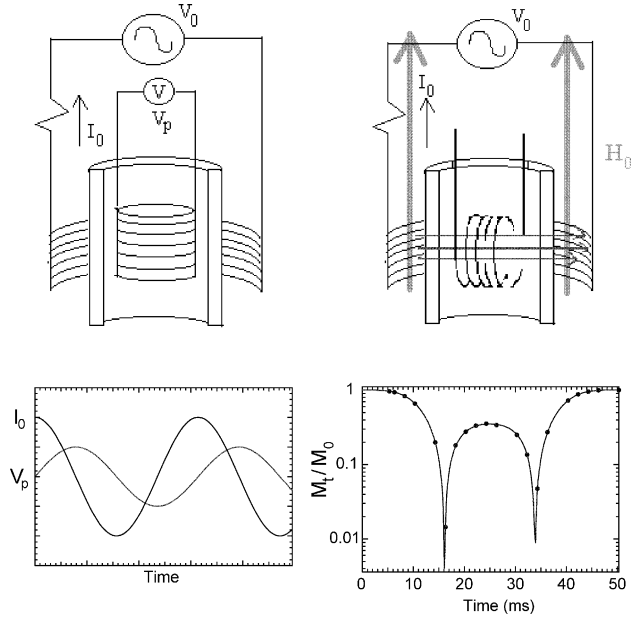

Fig. 1. Shielding measurement techniques. The inductive measurement is depicted on the left, where the shield's screening is measured through the pickup voltage on the inner coil from the outer coil's partially screened AC magnetic field. The NMR measurement, shown on the right as a function of Hahn echo formation time (2τ), measures the dephasing with signal averaging in a field ripple generated by the outer coil. The ^{1}H data shown was taken with a field ripple of 7.8 mG at 40 Hz.

Table 1
Shield properties (see text for discussion)

	Aluminum	OFHC copper
Radius R (mm)	10.9	16.5
Length l (mm)	50.8	96.6
Thickness t (mm)	2.45	5.23
ρ ($\mu\Omega$cm) @ 295 K	2.69	1.71
$\omega_{s,meas}/2\pi$(Hz) @ 295 K	430	86.0
$\omega_{s,calc}/2\pi$(Hz) @ 295 K	304	57.6
A (see Eq. (8))	1.19	1.15

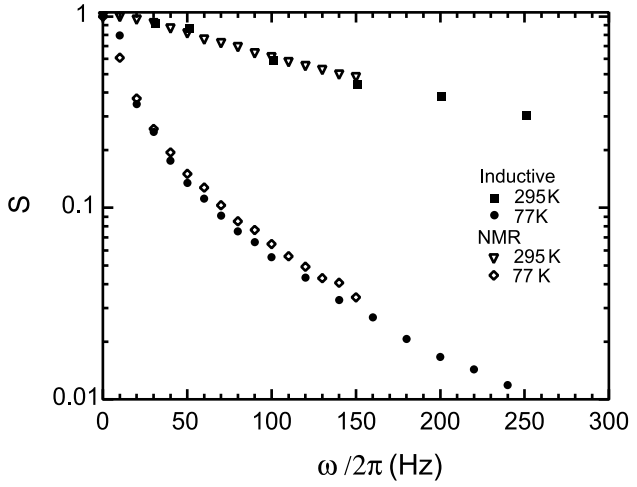

Fig. 2. OFHC Copper shield data. Inductive measurements: (■) 295 K; (●) 77 K. NMR measurements: (▽) 295 K; (◇) 77 K.

99.999% pure aluminum was machined to the maximal size for the Bitter magnet experiment geometry; it was chosen for this role due to its lower magnetoresistance at high fields compared to copper. It was then etched in an acid solution (phosphoric, sulfuric, and nitric), and annealed at 1 atmosphere at 620 °C for 25 h. The two classes of shielding measurement, inductive and NMR, were carried out on the copper shield, at two different shield temperatures of 295 and 77 K. The NMR measurements were performed with the ^{1}H resonance of glycerol at 3.15 T. The results are shown in Fig. 2. The agreement of the results of the two techniques is clear. NMR shielding measurements were also performed on the aluminum shield, and will be discussed in a later section.

3. Shielding calculation

We now turn to calculating the shielding fraction, for analysis of the experimental data. Qualitatively, we expect the shielding fraction at a given frequency ω is determined by how that frequency compares to the shield's "cutoff" frequency $\omega_s = r/L$, where r is the transverse resistance and L the inductance of the shield. This frequency scale, determined by shield geometry and resistivity, divides the frequency dependence of the shielding fraction into high- and low-frequency regimes. If we express this scale in terms of the parameters of a cylindrical shield (thickness t, radius R, length l, and resistivity ρ), and approximate (neglecting finite size effects) the inductance as $L = \mu_0 n^2 V$, where n is the turn density of the shield and V is its enclosed volume, we find,

$$\frac{\omega}{\omega_s} = \frac{\omega L}{r} \approx \frac{\omega\mu_0 \frac{1}{l^2}\pi R^2 l}{\rho \frac{2\pi R}{lt}} = tR\frac{\omega\mu_0}{2\rho} = \frac{tR}{\delta^2}, \tag{4}$$

where we recognize in the last step that the skin depth of the material $\delta \equiv \sqrt{2\rho/\omega\mu_0}$. Thus, the two regimes represent the limits of the skin depth of the shield material being long (low frequency) or short (high frequency) compared with the dimensions of the shield. The details of the shielding in each regime, and the crossover between them, are described below.

3.1. Low-frequency limit ($\omega \ll \omega_s$)

In the low-frequency limit, the skin depth is long compared with the shield dimensions, so the current density in the shield is roughly uniform, and we can treat it as a one-turn inductor. Kirchoff's laws can then easily be applied to determine the shielding fraction, as numerous authors have done for similar cases [3]. We calculated this case as a limiting case of a 3-coupled-inductor problem (applied field coil, pickup coil, and shield), with the result below.

$$S = \frac{1}{\sqrt{1 + \left(\frac{\omega}{\omega_s}\right)^2}} \quad (\omega \ll \omega_s). \tag{5}$$

Correction terms to the measured shielding fraction depending on the pickup coil were found to be important only for frequencies of the order of the pickup coil's r/L frequency, which was higher than ω_s, where the low-frequency approximation breaks down.

3.2. High-frequency limit ($\omega \gg \omega_s$)

In this limit, the skin depth is small compared with the shield dimensions, so we expect geometrical details to be less important in this regime. A first approximation to the shielding fraction might then be the attenuation of a plane wave EM field in an semi-infinite slab:

$$S = \exp(-t/\delta) = \exp\left(-\sqrt{\left(\frac{t}{R}\right)\left(\frac{\omega}{\omega_s}\right)}\right) \quad (\omega \gg \omega_s). \tag{6}$$

Here we have used the same first-order expression for the shield inductance as above. We see that the geometry

appears more explicitly in this limit beyond that in the cutoff frequency. Corrections to the self-inductance or transverse resistance calculations in Eq. (4) would modify both ω_s and the geometrical prefactor (in a non-cancelling way). However, the overall frequency dependence in this limit is well-defined for any shield.

3.3. Full frequency range

Finally, we show the result of an exact solution of Maxwell's equations for the cylindrical shield geometry [4] which describes the shielding fraction for arbitrary frequencies:

$$S = \left| \frac{2}{\alpha^2 b^2} \left[I_0(\alpha a) K_2(\alpha b) - K_0(\alpha a) I_2(\alpha b) \right]^{-1} \right| \tag{7}$$

where $\alpha \equiv (1+i)/\delta$, a and b are the outer and inner shield radii, respectively, and I_i, K_i are ith order modified Bessel functions. The frequency dependence for this formula and the limits previously described agree, i.e., either above or below $\omega/\omega_s \approx 1$.

In Fig. 3 we show a comparison of the experimental data for the copper shield from Fig. 1, as well as data from the aluminum shield. For each experimental data set, the frequency axis has been rescaled by a frequency ω_s to place it onto the "master curve" from the calculation of Eq. (7) for the appropriate shield geometry. The ω_s values obtained in this way are then converted to resistivities using Eq. (8) below, where a literature value

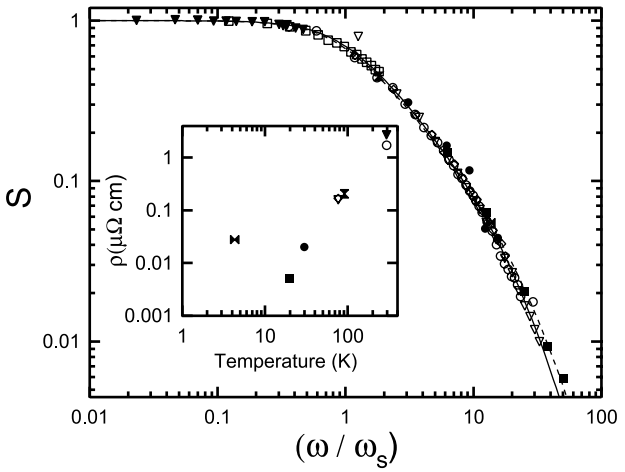

Fig. 3. Comparison of shielding data (by either NMR or *inductive* technique) with theory, at various temperatures and applied fields. Closed symbols: aluminum shield. Closed triangles, NMR, 295 K, 3.15 T; closed circles, NMR, 30 K, 3.15 T; closed squares, NMR, 20 K, 3.15 T; closed vertical bowtie, NMR, 91 K, 16.4 T; closed horizontal bowtie, NMR, 4.3 K, 22.1 T. Open symbols: OFHC copper shield. Open circles, *inductive*, 295 K, 0 T; open squares, NMR, 295 K, 3.15 T; open triangles, *inductive*, 77 K, 0 T; open diamonds, NMR, 77 K, 3.15 T. Lines: full calculation for each geometry: solid, copper shield; dashed, aluminum shield. Inset: resistivities extracted from matching shielding data to master curve. Symbols correspond to those in main figure.

[5] for the room temperature resistivity is used to determine the proportionality constant between ω_s and ρ. These resistivities are shown in the inset to Fig. 3. Table 1 shows, in addition to the shield geometries, the room temperature ρ and ω_s values for both shields. Also shown is a calculated prediction for ω_s, given $\rho(295\,\mathrm{K})$. This is found from

$$\omega_s = \frac{r}{L} = A\frac{2\rho}{\mu_0 t R} \tag{8}$$

as in Eq. (4), with a correction factor A, depending on the shield aspect ratio, for a finite-solenoid inductance [6]. The calculation compares fairly well with the experiment for both shields; the 30% discrepancy may be due to the assumption of a uniform current density along the length of the shield. In any case, the agreement between the full calculation of the shielding factor and the rescaled data from a large number of separate experiments is excellent. We make use of this well-defined behavior to better characterize the aluminum shield's performance in the Bitter magnets.

4. Bitter magnet shielding

High field NMR experiments were performed in resistive magnets at the National High Magnetic Field Laboratory in Tallahassee, Florida. In each experiment, the sample (glycerol) was held at room temperature, and the shield temperature varied with liquid helium or nitrogen. Hahn echo experiments were performed to measure the signal decoherence due to the applied field instability, and the reduction of this effect by the aluminum shield. Fig. 4 shows the results of one of these experiments, performed in Cell 9 of the NHMFL at $H_0 = 22.1$ T on the ^{13}C resonance in glycerol-$^{13}C_2$. First,

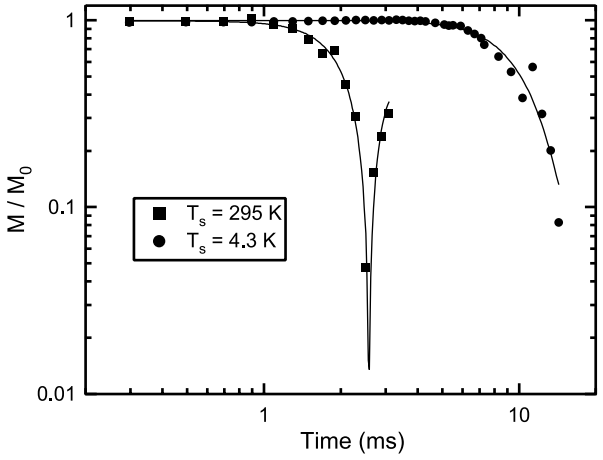

Fig. 4. NMR transverse magnetization decay profiles at $H_0 = 22$ T. Closed circles: 4.3 K shield. Closed squares: 295 K shield. Intrinsic decoherence has been divided out of these profiles. The shielding fraction was found to be $S = 0.055$.

a single acquisition at each echo time was recorded, mapping out the "single-shot" profile. This profile (not shown) is unaffected by phase noise reduction, since no signal averaging was performed, and it gives the intrinsic decoherence profile. The same experiment performed with signal averaging and a room temperature shield shows a pronounced decay due to phase noise, shortening the effective coherence time. Finally, the same experiment was performed with a room temperature sample and signal averaging, but with the shield cooled to 4.3 K with liquid helium. This reduced the magnetic field ripple, and extended the coherence of the signal by more than a factor of 4 towards the intrinsic profile. Fig. 4 shows both profiles acquired with signal averaging with the intrinsic profile (measured without averaging) divided out. The plateau of uncompromised magnetization measurement is clear.

Quantitatively, we can analyze the decay profiles with the model used to treat harmonic field variations, as we have done before [1]. This is given in Eq. (2), in terms of the amplitude h and frequency ω of a single harmonic ripple. The ripple spectrum is known to have a dominant 60 Hz component, so we fixed the harmonic frequency to 60 Hz in the fit in order to analyze the initial decay. Since the shield is essentially inactive at room temperature in this frequency range, the room temperature data fit gives the unshielded ripple magnitude of 1.86 ± 0.03 rms ppm, in good agreement with inductive measurements performed on Bitter style magnets by Brandt et al. (see [1]). The shielding factor for the 4.3 K shield was found to be $S = 0.055$. Shielding factors from two Bitter magnet experiments are shown in Fig. 3 (horizontal and vertical bowtie symbols) along with the other shielding data. We see from the corresponding resistivities that the ($T = 91$ K, $H_0 = 16.4$ T, $S = 0.45$) data is in keeping with the data trend, but the ($T = 4.3$ K, $H_0 = 22.1$ T, $S = 0.055$) resistivity seems higher by as much as a factor of 10 than the extrapolation of the other data. One explanation of this might be magnetoresistance, an effect that would only be apparent at low temperatures and high fields. Different effects might contribute to such a reduction in conductivity; a microscopic mechanism such as impurities or defects, as well as a macroscopic one like strong Lorentz forces from the magnet distorting the shielding current density from its ideal state. More experiments would have to be performed to distinguish between these two sources.

5. Conclusions

We have demonstrated that inductive shielding is a viable solution to the problem of magnetic field instability in the 60 Hz range in the Bitter magnets as applies to long timescale NMR measurements. After characterizing and optimizing the performance of an aluminum shield, we demonstrated suppression of the magnetic field ripple by a factor of $\sim$20 through a fully helium-cooled shield. This makes feasible a wider range of NMR experiments in the Bitter magnets (e.g., slow diffusion, long T_2) that require an extended magnetization coherence time with signal averaging.

Acknowledgments

We thank B. Brandt for many useful discussions. We also thank D. Seidman for valuable assistance in shield preparation and treatment.

References

[1] E.E. Sigmund, E.S. Calder, G.W. Thomas, V.F. Mitrović, H.N. Bachman, W.P. Halperin, P.L. Kuhns, A.P. Reyes, NMR phase noise in bitter magnets, J. Magn. Reson. 148 (2001) 309–313, doi:10.1006/jmre.2000.2246.

[2] V. Soghomonian, M. Sabo, A. Powell, P. Murphy, R. Rosanke, T.A. Cross, H.J. Schneider-Muntau, Identification and minimization of sources of temporal instabilities in high field (>23 T) resistive magnets, Rev. Sci. Inst. 71 (2000) 2882–2889.

[3] G. Planinšič, Shielding of low-frequency magnetic interference in weak-field MRI by a single-layer cylindrical coil, J. Magn. Reson. 126 (1997) 30–38.

[4] E.S. Meyer, I.F. Silvera, B. Brandt, Eddy current shielding and heating: Reduction of dissipation for very low-temperature experiments in the presence of magnetic field ripple, Rev. Sci. Inst. 60 (1989) 2964–2968;
S. Fahy, C. Kittel, S.G. Louis, Electromagnetic screening in metals, Am. J. Phys. 56 (1988) 989–992.

[5] G.W.C. Kaye, T.H. Laby, Table of Physical and Chemical Constants, Longmans Green, London, 1966.

[6] E.R. Cohen, The physics quick reference guide, American Institute of Physics (1996) 90–91.